www.springer.com/41230
https://doi.org/10.1007/s41230-026-5231-1

Influence of seed and crucible rotation on surface morphology during solution growth of 6-inch 4° off-axis SiC

Gang-qiang Liang[1], Jia-yi Kuang[1], Yi-lin Su[3], Ya-wei Chen[1], Jie Zhou[1], and *Yuan Liu[1, 2]

1. School of Materials, Tsinghua University, Beijing 100084, China

2. State Key Laboratory of New Ceramic Materials, Tsinghua University, Beijing 100084, China

3. TsingCheng Semiconductor, Suzhou 215127, Jiangsu, China

Copyright © 2026 Foundry Journal Agency

Abstract: The off-axis growth of SiC on C-face is strongly governed by seed or crucible rotation modes, exhibiting a specific surface step pattern. For unidirectional seed rotation, a macroscopic vortex-like pattern is observed across the entire crystal surface, corresponding to the flow field beneath the seed crystal. This results in macrosteps with heights reaching several millimeters. To suppress such surface roughening, the accelerated crucible rotation technique was applied to generate alternating azimuthal flow, producing antiparallel and parallel step-flow regions. However, this leads to anisotropy of the steps, with an increase in average step height from 5 μm to 170 μm along the [11–20] direction. To further reduce this step height discrepancy, switching rotation of both the seed and crucible was implemented, inducing alternating radial and azimuthal flows. This approach effectively decreases the average step height to approximately 30 μm.

Keywords: silicon carbide; top-seeded solution growth; surface morphology; step-flow growth

CLC numbers: TN305 **Document code:** A **Article ID:** 1672-6421(2026)06-849-08

1 Introduction

Silicon carbide (SiC), a wide-bandgap semiconductor with a bandgap of 3.2 eV (4H-SiC polytype), demonstrates exceptional material advantages over conventional silicon. Its wide-bandgap structure enables superior thermal stability (operating temperatures exceeding 300 °C) and high breakdown electric field (2–4 $MV \cdot cm^{-1}$)[1]. Combined with its outstanding thermal conductivity (4.9 $W \cdot cm^{-1} \cdot K^{-1}$, approximately three times that of silicon), these properties significantly reduce energy losses and improve heat dissipation in power devices. Furthermore, 4H-SiC exhibits remarkable electron saturation velocity (2×10^7 $cm \cdot s^{-1}$), making it particularly suitable for high-frequency applications. These physical advantages position 4H-SiC as a revolutionary semiconductor material capable of replacing silicon in power devices.

Unlike the Czochralski (Cz) method for silicon, SiC crystals cannot be grown by direct solidification from a stoichiometric SiC melt, as such a melt exists only under extreme high-temperature and high-pressure conditions. Solution growth provides an ideal approach for growing SiC bulk crystals from lower temperature (1,600–2,000 °C) and pressure (0.2–10 bar). The SiC solute dissolved by the Si-C-metal solution is supersaturated at the growth interface and then triggers the epitaxial growth. One of the most important advantages of the liquid phase growth of SiC is that it gives high-quality crystal since the growth proceeds under a condition close to the thermal equilibrium[2].

Typically, solution growth of SiC crystals is achieved through epitaxial growth on-axis or off-axis seed crystals. The solution growth on on-axis seed crystals is more conducive to achieve morphological stability. Nonetheless, epitaxial layer for SiC substrates is typically prepared via chemical vapor deposition (CVD), which requires substrates with a certain off-cut angle,

***Yuan Liu**

Male, born in 1974, Ph. D., Professor. His research interests mainly focus on semiconductor materials, porous metals, metallic composites for electronic packaging and advanced materials processing technology. He has been awarded the Excellent Young Talent Award of Chinese Mechanical Engineering Society (2015), Second Prize of Science and Technology Progress Award of Henan Province (2022), among others.

E-mail: yuanliu@mail.tsinghua.edu.cn

Received: 2025-09-22; Revised: 2025-10-19; Accepted: 2025-11-03

which is usually 4°[3, 4]. Therefore, on-axis SiC ingot required to be cut at an angle relative to the basal plane to produce off-axis substrates. This implies that a greater crystal thickness is required to yield off-axis substrates. For example, a 6-inch off-axis SiC substrate requires an on-axis ingot thickness of at least 11 mm. This significantly increases the production cost of P-type SiC substrates. Thus, achieving high-quality SiC crystal growth on off-axis seeds is critical for the mass production of off-axis P-type SiC substrates.

The off-axis seed crystals are usually cut with a 4° inclination from the (0001) plane toward the direction to facilitate step-controlled epitaxial growth, thereby maintain the stacking order of the desired polytype. However, growing SiC crystals on off-axis seeds via solution growth is challenging due to the frequent occurrence of step-bunching, which can lead to interfacial instability and solvent inclusions during growth[5, 6].

In solution-grown SiC crystals, step bunching often leads to macrostep collisions and trench-like defects, which induce solvent inclusions and basal plane dislocations (BPDs) within the crystal. Therefore, a rough crystal surface degrades crystal quality. A prerequisite for obtaining high-quality SiC crystals is maintaining fine step structures at solid-liquid interface during growth. Zhou et al.[7] numerically investigated the formation process of overhanging structures by phase-field simulations and demonstrated that overhanging inclusions could be suppressed by controlling the step height below 13 μm. Step height is influenced by factors such as carbon solubility in the solution[8-10], carbon diffusion coefficient[11-13], supersaturation[14-16], and interfacial energy[17-19].

Notably, in the growth of off-axis SiC crystals, the control of solution convection is one of the effective methods for reducing step height. Solution flow control can effectively suppress the step bunching during solution growth of SiC single crystals. Zhu et al.[20] grew 10 mm×10 mm 1° off-axis 4H-SiC single crystals and controlled step bunching by using parallel flow and anti-parallel flow. Dang et al.[21] first applied 3D simulation to investigate the effect of the crystal rotation speed on macrostep morphology, obtaining a 1.6 inches 1° off-axis 4H-SiC ingot. In this case, the experimental investigation on flow control for large-size (≥6 inches) 4° off-axis SiC crystals is rarely reported.

Hence, in this work, the effects of seed crystal rotation mode on the step behaviors of 6-inch 4° off-axis SiC bulk crystals in solution growth were systematically discussed, expecting to provide experimental guidance for growing large-size off-axis SiC crystals.

2 Numerical and experimental methods

As shown in Fig. 1, solution growth of SiC was performed in a top-seeded solution growth (TSSG) apparatus in argon atmosphere. 4° off-axis SiC (150 mm in diameter) was employed as the seed crystals. The rotation rates of the seed and crucible were controlled at 150 rpm (clockwise) and −20 rpm (counterclockwise), respectively. $Si_{45}Cr_{50}A_{15}$ mixture was melted in a graphite crucible under a pressure of 0.5 bar. During crystal growth, the temperature at seed crystals was kept at 1,820 °C. The height of the solution was 25 mm, the solution diameter was 270 mm. The growth period was 30 h. After growth for a duration of 30 h, the surface morphologies of the obtained SiC crystals were analyzed using a laser confocal microscope (LSM 900, Carl Zeiss AG, Germany).

To simulate the fluid flow, a two-dimensional axisymmetric model was established via COMSOL Multiphysics (Version 6.2) based on the coupling of electromagnetic field, heat transfer, and CFD. The turbulence induced by intensive forced convection from 150 rpm seed rotation was analyzed using the algebraic y^+ model, owing to its excellent robustness. Fine computational meshes were configured for both the solution and seed crystal domains. The maximum size of triangular meshed elements was set as 3 mm in solution domain (Fig. 1). To improve the computational accuracy, a 1 mm boundary layer adjacent to seed crystal and crucible wall was meshed using quadrangle elements and divided into 30 sublayers. The temperature of the water-cooled coil interface was set as 21 °C. The non-slip condition was applied to all solid-liquid interfaces, while the free surface of Si solvent was set as slip condition. The physical properties of materials are shown in Table 1.

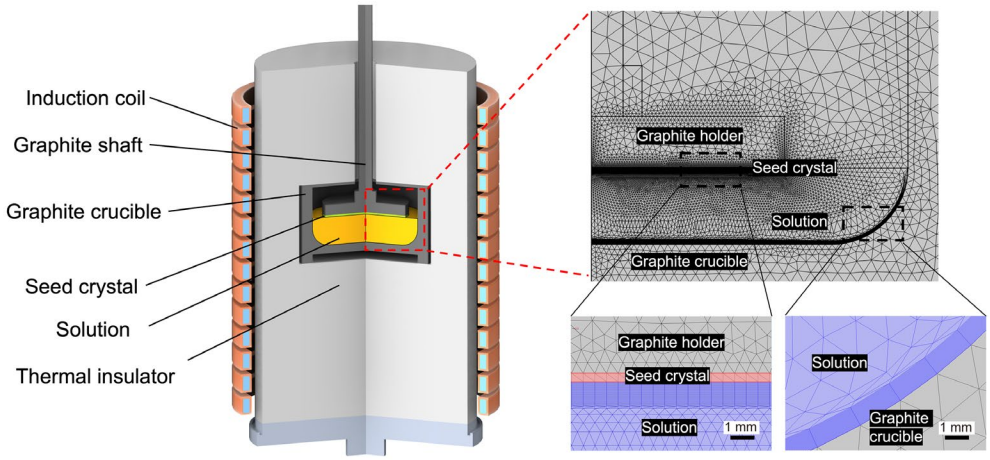


Fig. 1: Schematic illustration of the experimental apparatus for solution growth and mesh configuration for finite element analysis

Table 1: Physical properties of materials applied in CFD simulations[22-24]

Materials	Properties	Units	Equations/values
Solution	Thermal conductivity	$W·m^{-1}·K^{-1}$	$-68.28+5.4\times10^{-2}T$
	Electrical conductivity	$S·m^{-1}$	$2.21\times10^{6}-(2.8\times10^{9})T^{-1}$
	Density	$kg·m^{-3}$	$5199-0.552T$
	Surface tension coefficient	$N·m^{-1}·K^{-1}$	$1.195-1.23\times10^{-4}T$
	Viscosity	$Pa·s$	$1.266\times10^{-3}\exp(1982T^{-1})$
SiC seed crystal	Thermal conductivity	$W·m^{-1}·K^{-1}$	30
	Heat capacity	$J·kg^{-1}·K^{-1}$	1,290
	Surface emissivity	–	0.6
	Electrical conductivity	$S·m^{-1}$	225
Thermal insulator	Thermal conductivity	$W·m^{-1}·K^{-1}$	0.336
	Surface emissivity	–	0.6
	Heat capacity	$J·kg^{-1}·K^{-1}$	200
	Electrical conductivity	$S·m^{-1}$	430
Argon	Thermal conductivity	$W·m^{-1}·K^{-1}$	0.07
	Heat capacity	$J·kg^{-1}·K^{-1}$	520.33
	Electrical conductivity	$S·m^{-1}$	0
	Density	$kg·m^{-3}$	$552.21T^{-1}$
Graphite	Thermal conductivity	$W·m^{-1}·K^{-1}$	$150\times300T^{-1}$
	Heat capacity	$J·kg^{-1}·K^{-1}$	1,464
	Surface emissivity	–	0.8
	Density	$kg·m^{-3}$	1,830
	Electrical conductivity	$S·m^{-1}$	7.54×10^{4}

The temperature field is obtained by solving Fourier heat transfer equation and the expression is as follows:

$$\rho C_p u\cdot\nabla T-\nabla\cdot(k\nabla T)=Q_{in}+Q_{out} \quad (1)$$

where T denotes the temperature, ρ denotes the density, C_p denotes the specific heat capacity, u denotes the fluid velocity, k denotes the heat transfer coefficient, Q_{in} and Q_{out} denote the power of inter heater and outer heater, respectively.

In the high-temperature environment inside the resistance furnace, thermal radiation is the primary mode of heat transfer, described by the following equation:

$$G=G_m(J)+F_{amb}\sigma T_{amb}^4 \quad (2)$$

$$(1-\varepsilon_s)G=J-\varepsilon\sigma T^4 \quad (3)$$

$$\varepsilon_s(G-\sigma T^4)=-\boldsymbol{n}\cdot(-k\nabla T) \quad (4)$$

where G denotes the surface irradiation, G_m denotes the mutual surface irradiation, J denotes the surface radiosity, F_{amb} denotes the ambient view factor, σ denotes Stefan-Boltzmann constant, T_{amb} denotes the ambient temperature, ε_s denotes the surface emissivity, and $\boldsymbol{n}$ is the unit vector perpendicular to the crystal surface.

The flow of the solution is described by the Navier-Stokes equations as follows:

$$\begin{aligned}\varepsilon_s(G-\sigma T^4)&=-\boldsymbol{n}\cdot(-k\nabla T)\rho(u\cdot\nabla)u\\&=\nabla\cdot\left[-pI+\mu(\nabla u+(\nabla u)^T)\right]+\rho g\end{aligned} \quad (5)$$

$$\rho\nabla\cdot\boldsymbol{n}=0 \quad (6)$$

where I denotes the identity matrix, μ denotes the dynamic viscosity, g denotes the gravity.

3 Results and discussion

To study the effect of seed and crucible rotation on the surface morphology of off-axis SiC grown on the C-face, three rotation modes were employed [Figs. 2(a) to (c)], including the unidirectional rotation with the seed and crucible rotating in opposite directions; the accelerated crucible rotation technique (ACRT), where the seed and crucible are accelerated and deaccelerated while rotating in opposite directions; and the switching rotation, where the seed and crucible are alternately rotated.

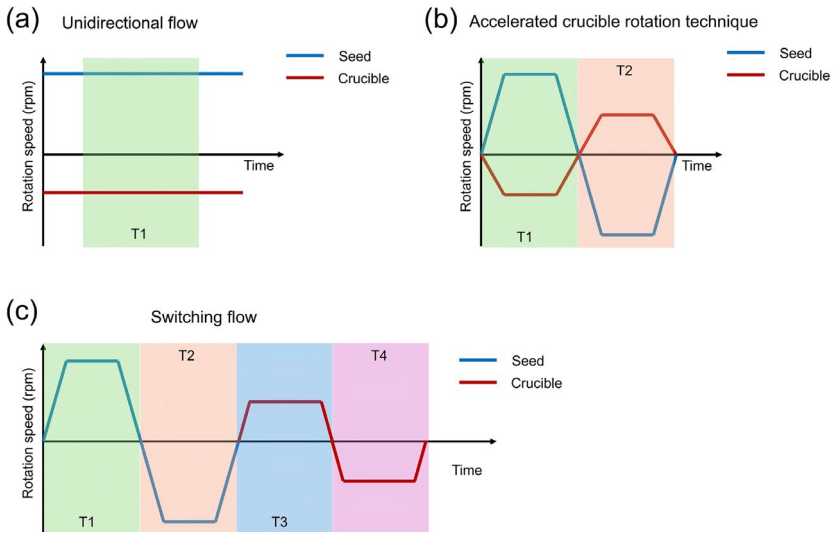


Fig. 2: Schematic of three rotation modes: (a) unidirectional rotation; (b) accelerated crucible rotation technique (ACRT); (c) switching rotation

To explain the flow under unidirectional rotation, ACRT, and switching rotation, CFD simulations were carried out, displaying the flow field on right half side of the solution, as shown in Figs. 3(a, b), and 0.5 mm beneath the seed, as indicated in Figs. 3(c, d). The flow velocity beneath the seed crystal can be decomposed into V_φ (azimuthal velocity, positive in the clockwise direction and negative otherwise) and V_r (radial velocity, positive outward along the radius and negative inward). Table 2 describes the change of V_φ and V_r under the three different rotation modes, where $T1$, $T2$, $T3$, and $T4$ denote the sub-period of the rotation mode.

As shown in Fig. 3(a), when the seed crystal rotates at ±150 rpm, the strong forced convection governs the flow pattern with a short solution height, resulting in the formation of a

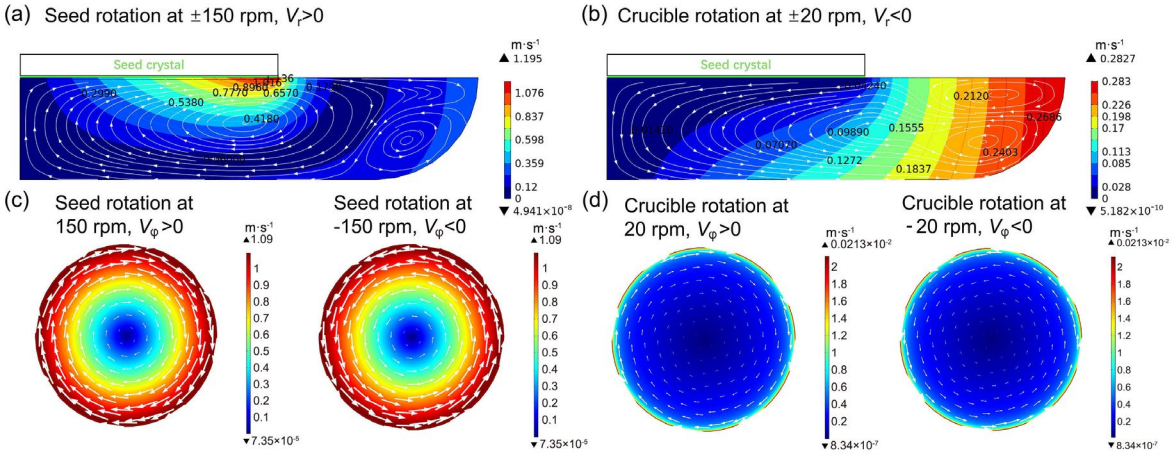


Fig. 3: Flow fields on right half side of the solution (a and b) and 0.5 mm beneath the seed (c and d) at various rotation rates

Table 2: Change of the azimuthal velocity V_φ and radial velocity V_r under unidirectional rotation, ACRT, and switching rotation

Rotation conditions	Change of V_φ and V_r			
Unidirectional rotation	$T1$ $V_\varphi>0$, $V_r>0$			
ACRT	$T1$ $V_\varphi>0$, $V_r>0$		$T2$ $V_\varphi<0$, $V_r>0$	
Switching rotation	$T1$ $V_\varphi>0$, $V_r>0$	$T2$ $V_\varphi<0$, $V_r>0$	$T3$ $V_\varphi<0$, $V_r>0$	$T4$ $V_\varphi<0$, $V_r>0$

double-vortex pattern. The large vortex in clockwise direction is induced by forced convection (V_r>0) and the small one is produced by Lorentz force. Even the crucible rotates at 20 rpm opposite to the seed rotation direction, the 150-rpm seed crystal rotation still governs the outward flow. By contrast, as shown in Fig. 3(b), when the crucible rotates at ±20 rpm without the seed crystal rotation, an inward flow formed under the seed crystal (V_r<0). Two minor vortices at the solution edge were respectively induced by Lorentz force. In Figs. 3(c) and (d), when seed crystal or crucible speed is positive, the V_φ defined as positive, and vice versa. The flow velocity is much lower under crucible-only rotation compared to seed-only rotation.

Under the conditions that seed crystal and crucible unidirectionally rotated at 150 and −20 rpm, respectively, the surface morphology of the crystal grown on a 4° off-axis substrate [Figs. 4(a) and (d)] exhibits a large vortex pattern on the entire crystal surface. This morphology aligns with the flow field distribution in the solution 500 μm beneath the seed crystal surface [Figs. 3(c) and (d)], indicating that the step-flow dynamics during off-axis growth is significantly influenced by the direction of convection.

As shown in Fig. 4(a), when V_r=0, the flow velocity at Point A on the seed crystal is parallel to the [1-100] direction, while the velocity at Point B is anti-parallel to the [1-100] direction. When V_r>0, Point A shifts upward to A', and Point B shifts downward to B', generating an azimuth angle θ. A'B' curve represents the isopleth when the solution flow velocity in the [11-20] direction is equal to 0 (flow velocity direction is parallel to [1-100] direction), which means that the flow has no contribution to anti-parallel flow and parallel flow. Consequently, regions above the A'B' curve exhibit flow velocity vectors parallel to the [11-20] direction, defining as the parallel flow region, where the steps are overlapped and rough. While regions below the A'B' curve exhibit velocity vectors anti-parallel to the [11-20] direction, which is defined as the anti-parallel flow region, where the large terraces are relatively smooth. The crystal surface morphology is rough under unidirectional flow, with macroscopic average step height of 2 mm observed. At the bends of these macro-steps, solvent inclusions are detected.

To eliminate severe step bunching caused by unidirectional rotation of seed crystals, ACRT [Fig. 2(b)] was applied to grow off-axis SiC crystal. In such rotation mode, periodic clockwise (V_φ>0) and counterclockwise (V_φ<0) convection occurs beneath the seed crystal. Shear forces at the solid-liquid interfaces (between the seed crystal or crucible and the solution) and within the fluid itself (inside the solution) enhance the mass transfer of carbon solute. Moreover, ACRT has been demonstrated as an effective method for accelerating crystal growth, attributed to the establishment of a larger concentration gradient at the growth interface and the homogenization of solutes within the boundary layer[25]. Figures 4(b) and (e) show that the surface morphology of the SiC grown crystals under ACRT results from the combined effects of the seed crystal's clockwise and counterclockwise rotations. The $-\theta$ azimuthal angle generated by the counterclockwise rotation compensates for the θ azimuthal angle produced by the clockwise rotation, facilitating uniform step advancement along the [11-20] step-flow direction across the entire seed crystal surface. Compared to unidirectional rotation, ACRT significantly smooths the surface morphology. Along the diameter line in the [1-100] direction, the surface is divided into two distinct regions: An anti-parallel flow region (left) and a parallel flow region (right). The step height and width exhibit noticeable variations along the [11-20] direction due to the different concentration gradient on the terrace and the step edge[20]. Overall, the surface

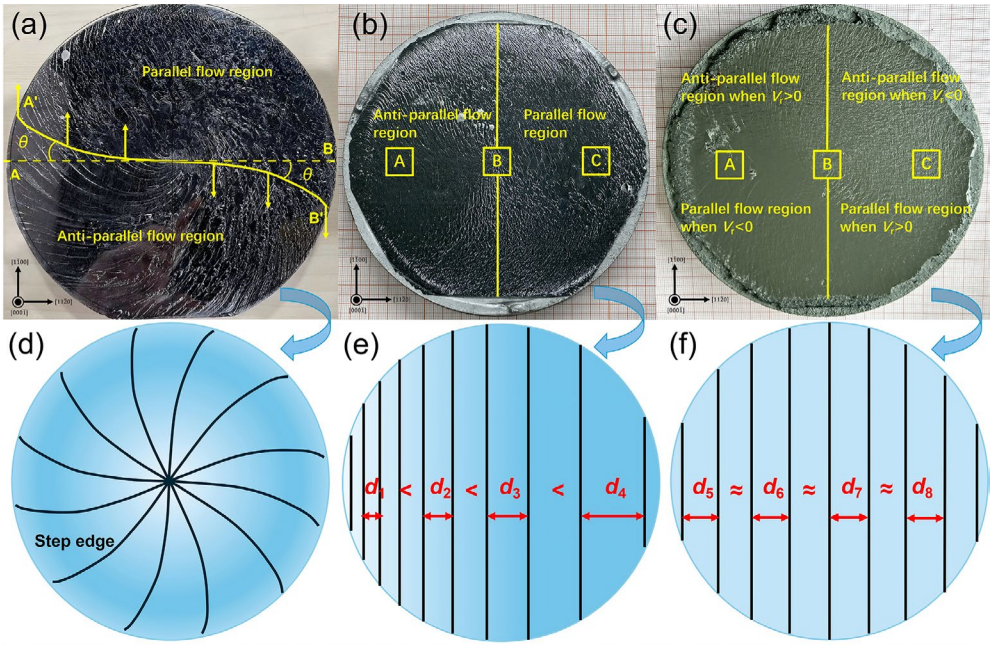


Fig. 4: Macroscopic surface morphologies of 4° off-axis SiC bulk crystal grown under unidirectional rotation (a), ACRT (b), and switching rotation (c), with seed crystal rotation at 150 rpm and crucible rotation at −20 rpm for 30 h at 1,820 °C, and schematic of surface step pattern under unidirectional rotation (d), ACRT (e), and switching rotation (f)

morphology is substantially smoothed, with a significant reduction in solvent attachment on the surface.

To homogenize step height and width along the [11-20] direction, a switching rotation strategy was employed. The rotational process is illustrated in Fig. 2(c). After the seed crystal completes one ACRT cycle, the crucible sequentially proceeds the next ACRT cycle. This approach aims to alternate the direction of V_r. During seed crystal rotation, centrifugal forces drive the melt flow, resulting in the outward flow (V_r>0). Similarly, when the crucible rotates, the inward flow (V_r>0) is achieved. When V_r>0, the left half of the region exhibits anti-parallel flow, while the right half exhibits parallel flow. Conversely, when V_r<0, the left half transitions to parallel flow, and the right half transitions to anti-parallel flow. The switching rotation mechanism alternates V_φ and V_r periodically, balancing the step variations induced by different rotation, which ultimately results in a uniform surface morphology. To quantify the effects of ACRT and switching rotation on the step morphology, optical and 3D reconstruction profiles were characterized at Positions A, B, and C in Figs. 4(b) and (c) by means of 3D laser confocal microscopy.

Figures 5(a) and (g) show Point A at the anti-parallel flow region under ACRT mode. The wandering narrow steps are observed. Moving to the central region of the crystal [Figs. 5(b) and (h)], Point B, the curvature of the step edge tends to decrease with expanding area of flat terrace. When it comes to the parallel flow region, surface roughening tends to increase along [11-20], in which the angle formed by the original growth surface and a faceted slope of large macro-steps is large, and a significant number of macro-steps with a terrace angle of 120° are frequently observed in the parallel flow region at Position C. This is because the solute concentration gradient near the edge of the macro-terrace is lower than that in front of the macro-step, leading to overlap of micro-steps on the macro-terrace. The formation of (10-1n) and (01-1n) facets drives the surface morphology to a more stable state, which pins the forward movement of macro-steps, thereby facilitating their further development by blocking the step flow from

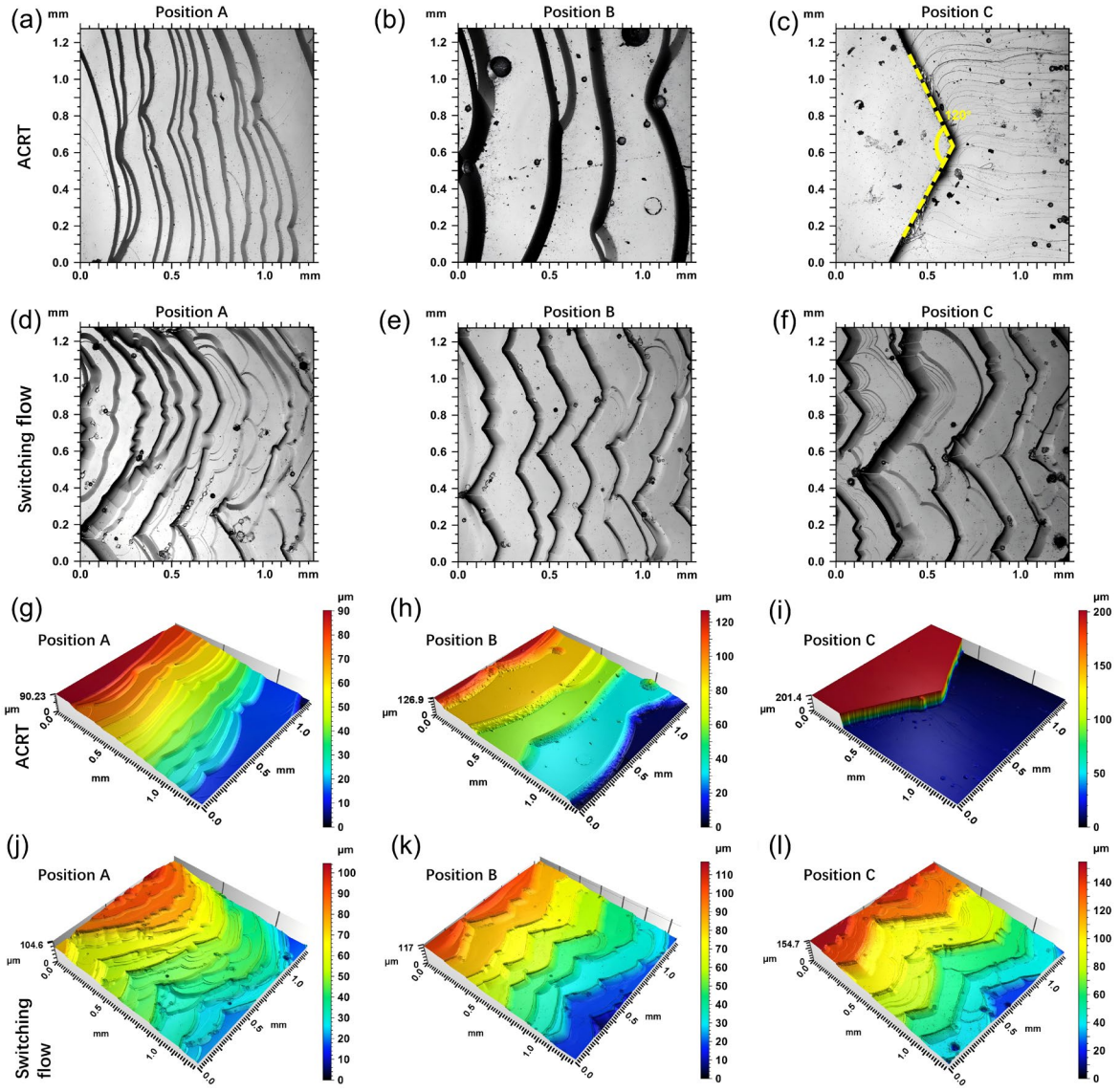


Fig. 5: 2D microscopic surface morphologies (a)–(f) and 3D step morphologies (g)–(l) of the surface of 4° off-axis SiC bulk crystals grown by ACRT (a)–(c), (g)–(i) and switching rotation (d)–(f), (j)–(l)

upstream[26-28]. Additionally, the pinning leads to the formation of a broad macro-terrace downstream. This step-faceting is an undesirable phenomenon for maintaining a flat growth interface in solution growth. As shown in Figs. 5(d), (e), and (f), the switching rotation alleviates the variation in step width along the [11-20] direction on the surface of SiC crystals. All steps exhibiting a zigzag morphology, which is composed of (10-1n) and (01-1n) facets. Step trains with narrow macro-terraces are observed. At Position C [Fig. 5(l)], the vicinal slopes decrease compared to those of ACRT.

Figure 6 depicts the section profiles of the average step height (H) and width (W) at Positions A, B, and C for ACRT and switching rotation samples, respectively. At Position A, the step dimensions produced by ACRT (H is ~5 μm, W is ~100 μm) are similar to those of the switching rotation steps (H is ~8 μm, W is ~100 μm), and small trenches are observed on the terraces of the switching rotation steps, resulting in minor measurement noise. At Position B, the ACRT steps increase significantly to H (~30 μm) and W (~300 μm), whereas the switching rotation steps remain more refined, with H (~15 μm) and W (~100 μm). At Position C, some degree of step coalescence is observed in the switching rotation sample, leading to an increase in H and W to approximately 40 μm and 200 μm, respectively, which are still smaller than the macro-steps produced by ACRT (H is ~170 μm, W is greater than 600 μm). These results indicate that, for off-axis growth, a smooth growth surface is achieved under the switching rotation.

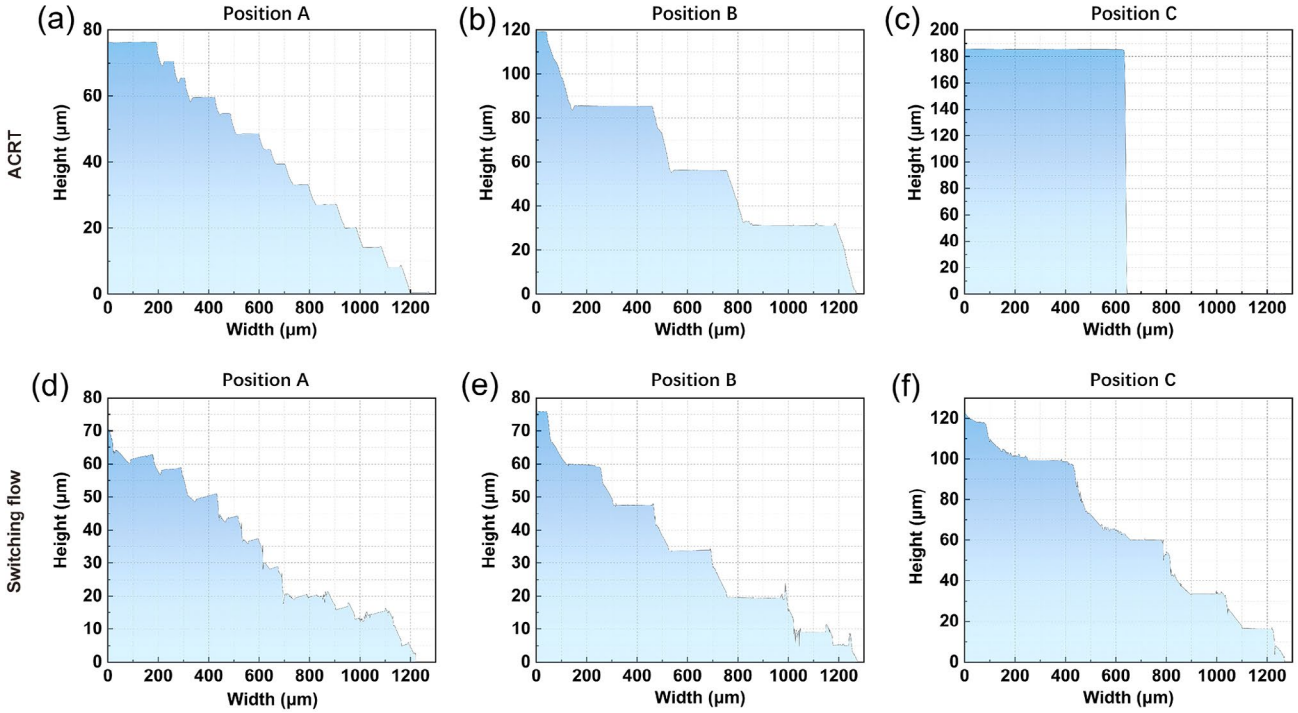


Fig. 6: Cross section of steps of 4° off-axis SiC bulk crystals grown by ACRT (a, b, c) and switching rotation (d, e, f)

4 Conclusions

This work discussed the effects of seed crystal and crucible rotation modes on the surface step pattern and micro-morphology during off-axis SiC crystal growth, including unidirectional seed crystal rotation, ACRT, and switching rotation. For optimizing the surface morphologies in SiC off-axial growth, the ACRT was applied to eliminate the rough morphology with a large vortex generated by the off-axis seed crystal's unidirectional rotation. However, it leads to a discrepancy in step height, with the step height and width gradually increasing along the [11-20] step flow direction. To deal with this, switching rotation of the seed and crucible supplies alternating flow in the radial and azimuthal directions. The switching rotation provides parallel and anti-parallel flow periodically, therefore, the height and width of the growth steps can be averaged. However, it is challengeable to obtain inclusion-free SiC crystals with zigzag-shaped microstructure in a long-term growth. Therefore, further efforts may focus on improving the surface morphological stability by realizing anti-parallel flow on the entire seed surface.

Acknowledgment

This work was supported by the Beijing Municipal Science and Technology Commission (Grant No. Z23111000270000).

Conflict of interest

Authors declare that they have no conflict of interest.

References

[1] Liang G Q, Qian H, Su Y L, et al. Review of solution growth techniques for 4H-SiC single crystal. China Foundry, 2023, 20(2): 159–178. https://doi.org/10.1007/s41230-023-2103-9.

[2] Liu X, Zhu C, Harada S, et al. Application of C-face dislocation conversion to 2 inch SiC crystal growth on an off-axis seed crystal. CrystEngComm, 2019, 21 (47): 7260–7265. https://doi.org/10.1039/c9ce01338e.
[3] Hattori R, Kusunoki K, Yashiro N, et al. Solution growth of off-axis 4H-SiC for power device application. Materials Science Forum, 2009, 600–603: 179–182. https://doi.org/10.4028/www.scientific.net/msf.600-603.179.
[4] Seki K, Kusunoki K, Harada S, et al. Evaluation of basal plane dislocation behavior in the epitaxial layer on a 4H-SiC wafer fabricated by the solution growth method. Materials Science Forum, 2019, 963: 80–84. https://doi.org/10.4028/www.scientific.net/MSF.963.80.
[5] Kamei K, Kusunoki K, Yashiro N, et al. Solution growth of single crystalline 6H, 4H-SiC using Si-Ti-C melt. Journal of Crystal Growth, 2009, 311(3): 855–858. https://doi.org/10.1016/j.jcrysgro.2008.09.142.
[6] Wang Y, Gu P, and Wang P. Improvement of surface morphology by optimizing the growth conditions in solution growth of SiC single crystal. Journal of Crystal Growth, 2023, 605: 127074. https://doi.org/10.1016/j.jcrysgro.2022.127074.
[7] Zhou H, Miura H, Dang Y, et al. Numerical simulation of the formation process of overhanging structures in SiC solution growth to suppress solvent inclusion. Crystal Growth & Design, 2025, 25(14): 5256–5264. https://doi.org/10.1021/acs.cgd.5c00314.
[8] Hyun K Y, Taishi T, Suzuki K, et al. Experimental determination of carbon solubility in $Si_{0.56}Cr_{0.4}M_{0.04}$ (M=transition metal) solvents for solution growth of SiC. Materials Science Forum, 2018, 924: 43–46. https://doi.org/10.4028/www.scientific.net/MSF.924.43.
[9] Hyun K, Kim S J, and Taishi T. Effect of cobalt addition to Si-Cr solvent in top-seeded solution growth. Applied Surface Science, 2020, 513: 145798. https://doi.org/10.1016/j.apsusc.2020.145798.
[10] Komatsu N, Mitani T, Hayashi Y, et al. Influence of additives on surface smoothness and polytype stability in solution growth of n-type 4H-SiC. Materials Science Forum, 2018, 924: 55–59. https://doi.org/10.4028/www.scientific.net/MSF.924.55.
[11] Zhou H, Miura H, Dang Y, et al. Numerical modeling of the cellular structure formation process in SiC solution growth for suppression of solvent inclusions. Crystal Growth & Design, 2023, 23(5): 3393–3401. https://doi.org/10.1021/acs.cgd.2c01512.
[12] Zhou H, Miura H, Fukami Y, et al. Effect of solution components on solvent inclusion in SiC solution growth. Crystal Growth & Design, 2024, 24(4): 1806–1817. https://doi.org/10.1021/acs.cgd.3c01476.
[13] Sheng D, Wang G, Yang Y, et al. Modeling and suppressing interfacial instability in growth of SiC from high-temperature solutions. Crystal Growth & Design, 2025, 25(4): 1211–1216. https://doi.org/10.1021/acs.cgd.4c01583.
[14] Komatsu N, Mitani T, Takahashi T, et al. Growth rate and surface morphology of 4H-SiC single crystal grown under various supersaturations using Si-C solution. Materials Science Forum, 2013, 740–742: 23–26.
[15] Li M, Liu Y, Qi X, et al. Suppression of the surface roughness by adjusting the temperature distribution in the top-seeded solution growth of SiC crystal. Journal of Materiomics, 2025, 11(5): 100994. https://doi.org/10.1016/j.jmat.2024.100994.
[16] Ha M T, Shin Y J, Lee M H, et al. Effects of the temperature gradient near the crystal-melt interface in top seeded solution growth of SiC crystal. Physica Status Solidi: A, 2018, 215(20): 1701017. https://doi.org/10.1002/pssa.201701017.
[17] Komatsu N, Mitani T, Hayashi Y, et al. Modification of the surface morphology of 4H-SiC by addition of Sn and Al in solution growth with SiCr solvents. Journal of Crystal Growth, 2017, 458: 37–43. https://doi.org/10.1016/j.jcrysgro.2016.10.045.
[18] Wang G, Sheng D, Li H, et al. Influence of interfacial energy on the growth of SiC single crystals from high temperature solutions. CrystEngComm, 2023, 25(4): 560–566. https://doi.org/10.1039/d2ce01500e.
[19] Liang G, Kuang J, Su Y, et al. Surface morphology of 6-inch SiC single crystals in solution growth on Si-face, C-face and (10-1-2) plane. Crystals, 2025, 15(5): 472. https://doi.org/10.3390/cryst15050472.
[20] Zhu C, Harada S, Seki K, et al. Influence of solution flow on step bunching in solution growth of SiC crystals. Crystal Growth & Design, 2013, 13(8): 3691–3696.
[21] Dang Y, Liu X, Zhu C, et al. Modeling-based design of the control pattern for uniform macrostep morphology in solution growth of SiC. Crystal Growth & Design, 2023, 23(2): 1023–1032.
[22] Daikoku H, Kawanishi S, Ishikawa T, et al. Density, surface tension, and viscosity of liquid Si-Cr alloys and influence on temperature and fluid flow during solution growth of SiC. Journal of Chemical Thermodynamics, 2021, 160: 106476. https://doi.org/10.1016/j.jct.2021.106476.
[23] Sui Z, Xu L, Cui C, et al. Effects of solution height and crystal rotation on the solution flow behavior in the top-seeded solution growth of SiC single crystals. CrystEngComm, 2024, 26(7): 1022–1031. https://doi.org/10.1039/d3ce01070h.
[24] Ha M T, Yu Y J, Shin Y J, et al. Flow modification enhancing the growth rate in top seeded solution growth of SiC crystals. RSC Advances, 2019, 9(45): 26327–26337. https://doi.org/10.1039/c9ra04930d.
[25] Kurashige K, Aoshima M, Takei K, et al. Effect of forced convection by crucible design in solution growth of SiC single crystal. Materials Science Forum, 2015, 821: 22–25. https://doi.org/10.4028/www.scientific.net/MSF.821-823.22.
[26] Nakanishi Y, Kutsukake K, Dang Y, et al. Analysis of macrostep interaction via carbon diffusion field in SiC solution growth. Journal of Crystal Growth, 2024, 631: 127609. https://doi.org/10.1016/j.jcrysgro.2024.127609.
[27] Kimoto T, Itoh A, Matsunami H, et al. Step bunching mechanism in chemical vapor deposition of 6H- and 4H-SiC {0001}. Journal of Applied Physics, 1997, 81(8): 3494–3500. https://doi.org/10.1063/1.365048.
[28] Daikoku H, Kawanishi S, and Yoshikawa T. Mechanism of replicating 4H-SiC polytype during solution growth on concave surface. Crystal Growth & Design, 2018, 18(7): 3820–3826. https://doi.org/10.1021/acs.cgd.8b00032.